Vibrational Feshbach resonances in near-threshold HOCO^{-} photodetachment: A theoretical study

S. Miyabe, D. J. Haxton, K. V. Lawler, A. E. Orel, C. W. McCurdy, and T. N. Rescigno

Phys. Rev. A **83**, 043401 — Published 1 April 2011

DOI: 10.1103/PhysRevA.83.043401

Vibrational Feshbach resonances in near threshold $HOCO^-$ photodetachment; a theoretical study

S. Miyabe,[1,2] D.J. Haxton,[1] K.V. Lawler,[1] A.E. Orel,[3] C.W. McCurdy,[1,4] and T. N. Rescigno[1]

[1]*Lawrence Berkeley National Laboratory, Chemical Sciences, Berkeley, CA 94720*
[2]*Department of Chemistry, University of California, Davis, CA 95616*
[3]*Department of Applied Science, University of California, Davis, CA 95616*
[4]*Departments of Chemistry and Applied Science, University of California, Davis, CA 95616*

The results of a theoretical study of $HOCO^-$ photodetachment are presented, with a view toward understanding the origin of two peaks observed by Lu and Continetti (Phys. Rev. Lett. 99, 113005 (2007)) in the photoelectron kinetic energy spectrum very close to threshold. It is shown that the peaks can be attributed to vibrational Feshbach resonances of dipole-bound trans-$HOCO^-$, and not s- and p-wave shape resonances as previously assumed. Fixed-nuclei variational electron-HOCO scattering calculations are used to compute photodetachment cross sections and laboratory-frame photoelectron angular distributions. The calculations show a broad $A''(\pi^*)$-shape resonance several eV above threshold.

I. INTRODUCTION

The bimolecular reaction between the hydroxyl radical and carbon monoxide, $OH+CO \rightarrow H+CO_2$, is important in atmospheric and combustion chemistry. As an intermediate, the HOCO radical governs the dynamics of this process. For this reason, there has been a considerable amount of experimental and theoretical study aimed at characterizing the molecule [1–3]. The $HOCO^-$ anion, which can be formed during the reaction of OH^- + CO in a supersonic expansion, has also been the subject of theoretical [4, 5] and experimental study. Clements *et al*[6] and Lu *et al.*[7] showed that the dissociative photodetachment of the anion provides insight into the potential energy surface of HOCO and the dynamics of the combustion reaction. More recently, Lu and Continetti [8] studied the threshold detachment region with 1.60 eV photons and found two sharp peaks in the distribution of photejected electrons at 0.01 eV and 0.09eV, which they interpreted as s- and p-wave shape resonances, respectively, based largely on the angular distributions associated with the two features(see Fig. 1). They showed that the latter feature could be used to align the molecular anion by a two-photon detachment process.

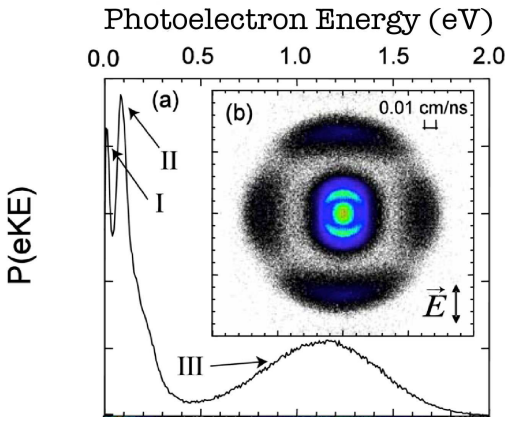

FIG. 1: (Color online) $HOCO^-$ photoelectron detachment spectrum at $E_{h\nu}$=1.6 eV from Lu and Continetti [8]. (a) Angle-integrated spectrum. Note that peak (III) comes from 2-photon absorption. (b) 2D projection of 3D laboratory-frame photoelectron angular distributions.

The assignment of the threshold peaks as shape resonances was based on an atomic approximation for photodetachment in which the interaction between the photoelectron and the neutral molecular core is assumed to be of short range, i.e., to fall off faster than r^{-2} at large distances. An important factor not considered in this interpretation is the permanent dipole moment of the molecule. For molecules with strong permanent dipole moments the properties of the ejected electron are influenced by the dipole field, which is long-range in nature and strongly mixes continuum partial-waves. Because of this mixing, one would not expect for find narrow shape resonances close to threshold. Molecules with sufficiently large dipole moments can bind an electron. Indeed, binding of an electron to the dipole field of a polar molecule is a well known phenomenon. Dipole-bound states are observed in various experiments and their existence is supported by *ab initio* calculations [9–11]. Rohr and Linder studied the scattering of low energy electrons by HF and HCl and found resonance structure at the vibrational thresholds. The resonances have been ascribed to a temporary binding of an electron to the dipole field of the molecule [12, 13]. Dipole-bound states are also observed in the photodetachment spectrum of various anions [14–18]. Zimmerman *et al*. were one of the first groups to observe sharp resonances in the photoelectron spectrum of the acetophenone enolate anion [14]. They attributed the resonances to the vibrational levels of the dipole-bound anion. More recently, dipole-bound states have been attributed to a series of sharp peaks in the dissociative electron attachment cross sections of DNA bases, RNA base uracil, and the halouracils [19–22]. Similarly, here it will be shown that a dipole-bound state offers a more plausible explanation for the threshold peaks seen in the

photoelectron energy distribution of $HOCO^-$ than electron scattering shape resonances. Our calculations will show that these resonances result from excitation of the OCO bend vibrational motion in the dipole-bound anion. The electronic structure theory of dipole-bound states is well established [11, 23–28] and will be used to aid the analysis.

We will also present photodetachment cross sections obtained from variational, fixed-nuclei scattering calculations. While these calculations show no evidence of any threshold peaks, they do identify a shape resonance several eV above threshold with dominant contributions from l=1 and l=2 partial waves. Laboratory-frame photoelectron angular distributions will also be presented.

II. COMPLEX-KOHN CALCULATION: PHOTODETACHMENT CROSS SECTION OF $HOCO^-$

Photodetachment of a molecular anion at a fixed photon frequency can in general produce photoelectrons – and corresponding rovibrational states of the neutral molecule – over a range of energies that span the Franck-Condon region of the initial anion. However, in the scattering calculations we report here, the nuclei were constrained to be fixed at the equilibrium geometry of the anion, and so we have, in our calculations, a one-to-one correspondence between photon energy and photoelectron energy. Fixed-nuclei photodetachment amplitudes were computed using the complex Kohn variational method[29, 30]. Since the method does not rely on single-center expansions to compute the required electron-moelcule continuum wavefunctions, it is well suited to applications involving polyatomic targets. Here we give a brief summary. The final-state wave function for production of a neutral molecule in a specific state Γ_0 is written as

$$\Psi^-_{\Gamma_0} = \sum_{\Gamma} A(\chi_\Gamma F^-_{\Gamma\Gamma_0}) \tag{1}$$

where Γ labels the final target states χ_Γ included, $F^-_{\Gamma\Gamma_0}$ are channel functions that describe the photodetached electron, and A is the antisymmetrization operator. Note that we are using Γ_0 as a combined index to denote the target electronic state and the angular momentum quantum numbers l_0, m_0 of the ejected photoelectron.

In the Kohn method, the channel functions are further expanded, in the molecular-frame, as

$$\begin{aligned} F^-_{\Gamma\Gamma_0}(\mathbf{r}) = &\sum_i c_i^{\Gamma\Gamma_0}\varphi_i(\mathbf{r}) \\ &+ \sum_{lm}\Big[f_{lm}(k_\Gamma, r)\delta_{ll_0}\delta_{mm_0}\delta_{\Gamma\Gamma_0} \\ &+ T^{\Gamma\Gamma_0}_{ll_0mm_0} g^-_{lm}(k_\Gamma, r)\Big] Y_{lm}(\hat{\mathbf{r}})/k_\Gamma^{\frac{1}{2}} r\,, \end{aligned} \tag{2}$$

where the $\varphi_i(\mathbf{r})$ are a set of square-integrable (Cartesian Gaussian) functions, Y_{lm} is a normalized spherical harmonic, k_Γ are channel momenta, and the $f_{lm}(k_\Gamma, \mathbf{r})$ and $g^-_{lm}(k_\Gamma, \mathbf{r})$ are numerical continuum functions that behave asymptotically as regular and incoming Riccati-Bessel functions, respectively.[31] The coefficients $T^{\Gamma\Gamma_0}_{ll_0mm_0}$ are the T-matrix elements.

Photodetachment cross sections can be constructed from the matrix elements

$$I^\mu_{\Gamma_0} = < \Psi^-_{\Gamma_0} | r_\mu | \Psi_0 > , \tag{3}$$

where r_μ is a component of the dipole operator, which we evaluate here in the length form,

$$r_\mu = \begin{cases} z, & \mu = 0 \\ \mp (x \pm iy)/\sqrt{2}, & \mu = \pm 1 \end{cases} \tag{4}$$

and Ψ_0 is the initial state wave function of the target molecular anion. To construct an amplitude that represents a photoelectron with momentum $\mathbf{k}_{\Gamma_0}$ ejected by absorption of a photon with polarization direction $\hat{\epsilon}$, measured relative to the molecular body-frame, the matrix elements $I^\mu_{\Gamma_0}$ must be combined in a partial wave series:

$$I_{\mathbf{k}_{\Gamma_0},\hat{\epsilon}} = \sqrt{\frac{4\pi}{3}} \sum_{\mu l_0 m_0} i^{-l_0} I^\mu_{\Gamma_0} Y_{1\mu}(\hat{\epsilon}) Y_{l_0 m_0}(\hat{k}_{\Gamma_0})\,. \tag{5}$$

The cross section, differential in the angle of photoejection and photon polarization relative to the fixed body-frame of the molecule, is then given (in atomic units) by

$$\frac{d^2\sigma}{d\Omega_{\hat{k}_{\Gamma_0}} d\Omega_{\hat{\epsilon}}} = \frac{8\pi\omega}{3c} |I_{\mathbf{k}_{\Gamma_0},\hat{\epsilon}}|^2\,, \tag{6}$$

where ω is the photon energy and c is the speed of light. To compute a laboratory frame photoelectron angular distribution Eq. (6) is averaged over all orientations of the target anion. The resulting differential cross section has the form

$$\frac{d\sigma^{\Gamma_0}}{d\Omega} = \left\langle \frac{d^2\sigma}{d\Omega_{\hat{k}_{\Gamma_0}} d\Omega_{\hat{\epsilon}}} \right\rangle_{av} = \frac{\sigma^{\Gamma_0}}{4\pi}[1 + \beta^{\Gamma_0} P_2(cos\theta)]\,, \tag{7}$$

where P_2 is the Legendre polynomial of order 2, θ is the angle between $\hat{\epsilon}$ and $\hat{k}$ and β^{Γ_0} is the asymmetry parameter. The photodetachment total cross section is obtained by averaging over polarization directions and integrating over photoelectron directions and is given by

$$\sigma^{\Gamma_0} = \frac{8\pi\omega}{3c} \sum_{l_0 m_0 \mu} |I^\mu_{\Gamma_0}|^2\,. \tag{8}$$

III. RESULTS

A. Photodetachment cross sections

The square-integrable portion of the basis for the complex Kohn calculations consisted of Dunning's triple-zeta

basis [32], augmented with one p-type and one s-type function on all atoms. To this set, 5 s-type, 5 p-type and 4 d-type functions were added at the center of mass. In addition, numerical continuum functions up to l=6 and m=6 were included.

To avoid working with non-orthogonal orbitals, a single set of molecular orbitals is used to construct both the initial anion and final neutral states. Those orbitals can be obtained from calculations on the target anion, the neutral molecule or some average of the two. That choice can strongly affect the computed cross sections and, in particular, the positions and widths of shape resonances. For example, in C 1s photoionization of neutral CO_2, the cross sections computed using the ion molecular orbitals or averaged (Slater's transition-state [33]) orbitals give much better agreement with experimental observations than those obtained with CO_2 molecular orbitals[34–36]. Slater's transition-state orbitals have been used extensively in core-level photoionization studies and have been shown to give results consistent with experimental measurements[34, 35, 37, 38]. To investigate the orbital relaxation effects in the case of photodetachment, here we compute the cross sections using anion, neutral and Slater's transition-state orbitals. The latter is obtained by taking the average of the anion and neutral orbitals using natural orbital techniques.

The total photodetachment cross sections of trans-$HOCO^-$, calculated using the three types of molecular orbitals, are plotted in Fig. 2. The calculation is done at the equilibrium geometry of $HOCO^-$ computed by Clements et al [6]. Clearly, the position of the resonance shifts to lower energy and the magnitude increases as the orbitals used in the calculation become more anionic. The cross section for cis-$HOCO^-$, obtained using the anion orbitals, is shown in the same figure and it is very similar to that of the trans-conformer. The similarity between cis- and trans-conformer cross sections holds for other orbital choices as well. From here on, we will focus on the trans-$HOCO^-$ results obtained with transition-state orbitals.

There have been no experimental measurements of the electron affinity of HOCO, although theoretical calculations [4, 6] indicate that it requires ∼1.4 eV to detach an electron from the valence shell of $HOCO^-$. The experiment of Lu and Continetti [8], which used a fixed photon energy of 1.60 eV, could therefore only probe photoelectrons up to a few tenths of an eV produced by single photon absorption. The broad peak in their measured photoelectron spectrum (labeled III in Fig. 1) centered near 1.2 eV comes from 2-photon absorption and is therefore not directly related to our calculated single-photon detachment cross section. Of more relevance to the present calculations are the earlier measurements of Clements *et al* [6] and Lu *et al* [7] done at 4.80 eV and 3.21 eV photon energy, respectively. These experiments showed the photoelectron peaks corresponding to e^- + HOCO production centered at 2.7 eV and 1.3 eV, respectively. If there were no resonance involved, one would expect the

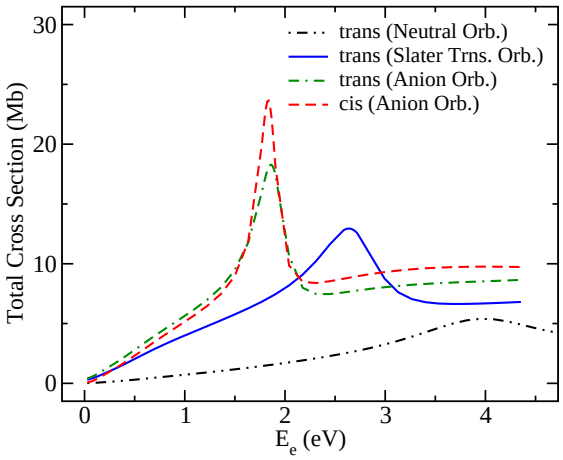

FIG. 2: (Color online) Total photodetachment cross section, as a function of photoelectron energy, for trans-$HOCO^-$ calculated using the neutral, Slater's transition-state, and anion orbitals. The cross section for cis-$HOCO^-$ computed using anion orbitals is also shown.

difference in the peak positions to simply correspond to the difference in photon energies, i.e., 4.80 - 3.21 = 1.59 eV, instead of the observed value of 1.4 eV. The observation is consistent with the $E_{h\nu}$=4.80 eV measurement probing a resonance near 2.7 eV, which would shift the peak down from the expected value of 2.89 eV (i.e. 1.3 + 1.59 eV) and which is consistent with our calculations that use transition-state orbitals and show a resonance near 2.7 eV.

$HOCO^-$ is planar, so the calculations were carried out in C_s symmetry for the A′ and A″ components of total photodetachment cross section. In Fig. 3 the partial photodetachment cross sections for trans-$HOCO^-$, computed using transition-state orbitals, are presented. The figure shows an A″ shape resonance with a maximum at around E_e= 2.7 eV, while the A′ component of the cross section varies slowly with energy. The calculations clearly identify the 2.7 eV feature as an out-of-plane, π^* shape resonance.

To investigate the origin of the shape resonance in more detail, the plots of the partial cross sections of trans-$HOCO^-$, summed over the m quantum numbers and averaged over polarization directions, are shown in Fig. 4a. The importance of the centrifugal term in the potential is clearly shown. Our calculation shows the dominance of s-wave contributions very near threshold. This is also shown by the laboratory-frame angular distribution and the beta parameter at those energies. The beta parameter, shown in Fig 4b, approaches zero at very low energies. The angular distributions are shown in Fig 5a, and they become more isotropic as energy decreases, which is consistent with the observations of Lu and Continetti [8]. The $l = 1$ contribution quickly becomes the dominant component as the photoelectron energy increases, leading to a characteristic dipole pattern in the angular distribu-

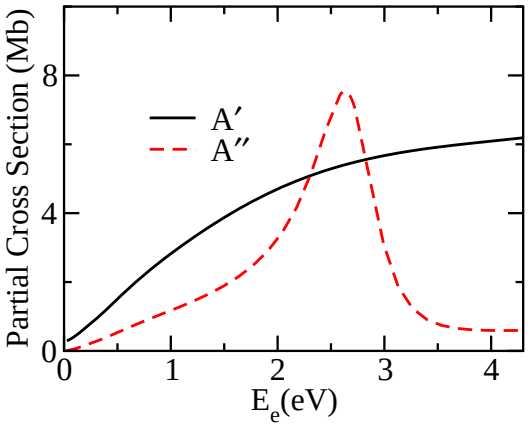

FIG. 3: (Color online) A′ and A″ components of the photodetachment cross section for trans-HOCO$^-$ calculated using transition-state orbitals.

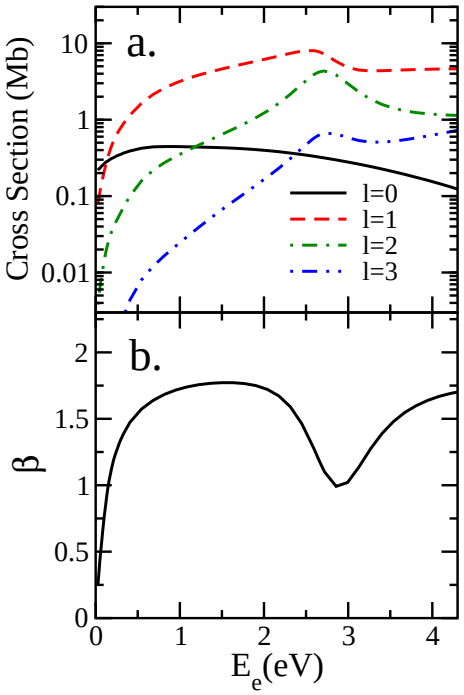

FIG. 4: (Color online) a) Parital photodetachment cross section for trans-HOCO$^-$ summed over quantum number m. b) Beta parameter for trans-HOCO$^-$. The calculations are done using transition-state orbitals.

tion, except near the resonance peak, where the $l = 1$ and $l = 2$ partial wave contributions become comparable. There is also a very small contribution from l=3. As expected the beta parameter changes rapidly as the energy goes through the resonance region. The change is demonstrated by the angular distributions plotted in Fig 5b. Although the angular distributions near threshold are consistent with experiment, the calculations do not

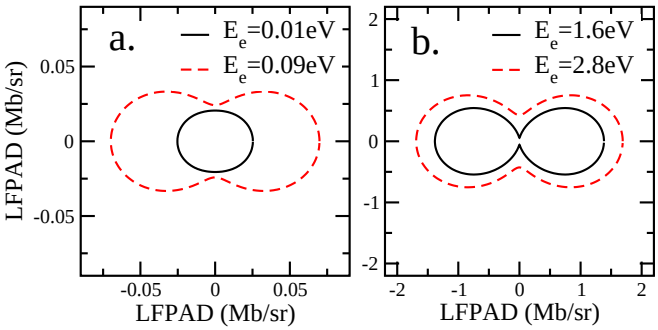

FIG. 5: (Color online) a) Near threshold laboratory frame photoelectron angular distributions for trans-HOCO$^-$. b) The distributions plotted near the resonance energy.

show peaks near threshold, leading us to conclude that peaks (I) and (II) observed by Lu and Continetti cannot be shape resonances.

B. Dipole supported states; Vibrational Feshbach resonances in HOCO$^-$ photodetachment

Fermi and Teller [39] were the first to show that a non-rotating dipole with magnitude d>1.625 D can support an electron in an infinite number of bound states. A number of subsequent studies demonstrated that, even in the low temperature limit, rotational motion becomes important and the critical dipole-moment and the number of bound states depend on the moment of inertia of the molecule [40, 41]. For small molecules, Garret [40] has provided the rough rule of thumb that a dipole moment must be greater than 2.0D to bind an electron by one meV or more.

With small, non-polar closed-shell neutral molecules, the lowest valence unoccupied molecular orbital (LUMO) typically lies in the continuum, so the associated "anion" exists as a transient state that can be observed as a resonance in electron-neutral molecule scattering cross sections. With open-shell neutral molecules, stable valence-bound anions often exist, with electron binding energies typically less than 3 eV. When the open-shell neutral molecule has a large permanent dipole moment, it may support *both* a valence anion and an excited, dipole-bound anion [25]. The dipole-bound anion is analogous to a highly excited Rydberg state of a neutral molecule, where the electron is weakly bound in a diffuse orbital and the nuclear geometry is very much like that of the cationic, or in the dipole-bound case, the neutral core. Since the binding energies of dipole-bound states are typically on the order of a few meV, their vibrationally excited states can autodetach into the neutral plus free electron continuum and can be detected experimentally as sharp resonances in the near-threshold photodetachment cross section.

Dipole-bound states have been accurately described

using various bound-state methods. Wetmore *et al* [23] investigated the electronic structure of the acetaldehyde enolate anion at the SCF level and demonstrated that there was a Rydberg-like state of the anion whose properties are very similar to the ground-state of the neutral. They pointed out the possibility that vibrationally excited levels of this dipole-bound state could be responsible for the sharp resonances observed in electron photodetachment experiments. Gutowski *et al*. [24] later included electron correlation in the description by means of the coupled-cluster method with single, double, and noniterative triple excitations [CCSD(t)]. A number of other groups[25–28] have successfully calculated the properties of these states. Electron correlation is known to affect the binding energy of dipole-bound states in two opposing ways: 1) the electron correlation in many cases decreases the dipole moment and hence the binding energy, and 2) assuming electron correlation has little affect on the dipole-moment, there are other correlation effects that actually increase the binding energy. Here the binding energies are computed at the SCF and configuration-interaction level of theory with single and double excitations (CISD). In addition, dipole moments are computed at the SCF and MP2 level using the Gaussian 09[42] package.

Previous investigations show that the most important requirement in describing dipole-bound anions is the inclusion of diffuse functions capable of describing the highest occupied molecular orbital (HOMO) that localizes most of its density behind the positive end of the molecule[23]. This can be accomplished by including diffuse s- and p- atom-centered basis functions on the electropositive atom(s). All the calculations presented here are done using the Dunning's triple-zeta Gaussian-orbital basis set [32], supplemented with a large set of diffuse primitive Gaussian functions centered on the hydrogen and carbon atoms. The exponents of the added eight s- and p- functions form an even-tempered sequence, with the ratio between exponents being 3.2. The smallest exponent of the added s- and p- functions was 2.0 x 10^{-5}.

The MP2 calculations gave values of 2.84 D and 1.86 D for the dipole-moment of trans- and cis-HOCO, respectively. The dipole field of trans-HOCO is strong and it should be able to bind an electron, while the potential of cis-HOCO is too weak. At the SCF level, the dipole moments of trans- and cis- HOCO are 3.55 D and 1.98 D, respectively. Clearly, electron correlation decreases the dipole moment. The HOMO of trans-$HOCO^-$ from an SCF calculation on the triplet state of the anion is shown in Fig. 6 and it shows the majority of density being concentrated behind the positive end of the molecule, in agreement with previous observations. Koopman's theorem gives a binding energy of 3.2 meV, while at the CISD level of theory, the binding energy of the anion is 0.48 meV. In the latter calculation, the desired value was obtained by subtracting the energy computed for the anion from that of neutral. Consistent with previous observations, electron correlation decreases the dipole moment

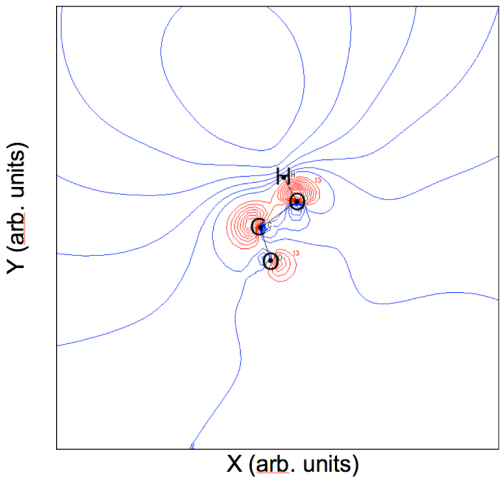

FIG. 6: (Color online) Contour plot of the HOMO of trans-$HOCO^-$ from our SCF calculation. Blue and red lines correspond to regions of positive and negative values, respectively, of the orbital.

and as a consequence the binding energy goes down. All calculations suggest that trans-HOCO can bind an electron to form a stable dipole-bound anion.

Our calculations suggest that the threshold peaks observed in the photoelectron spectrum can be ascribed to the decay of a vibrationally excited level of the dipole-bound trans-$HOCO^-$. The experiment was performed with a fixed photon frequency of 1.6 eV. If we assume that the ground state of trans-$HOCO^-$ is bound by 1.4 eV, then the vibrationally excited level of the dipole-bound state that is populated in the experiment must lie ∼0.2 eV above the detachment threshold. Since the outer electron in dipole-bound $HOCO^-$ occupies a region of space far from the neutral HOCO core, it is reasonable to assume the vibrational frequencies of dipole-bound $HOCO^-$ and trans-HOCO to be very similar. The vibrational energy spacing between the OCO bend levels in trans-HOCO is 0.08 eV [43], which is also the spacing between the threshold photodetachment peaks observed by Lu and Continetti [8].

The mechanism these calculations suggest is responsible for the threshold peaks is that a 1.6 eV photon populates the $\nu_f = 2$ OCO bend level of the dipole-bound anion, which then autodetaches to leave neutral HOCO in either its ground or first excited vibrational levels, producing photoelectrons near zero and 0.08 eV, respectively. To verify that this mechanism is plausible we must first consider the Franck-Condon approximation for the transition to the $\nu = 2$ level of the OCO bending mode, and then examine the potential curves of the dipole bound anion for that vibrational mode.

While the potential energy surfaces of the dipole-bound anion and neutral HOCO are expected to be very similar, the potential energy surfaces of ground-state $HOCO^-$ and dipole-bound $HOCO^-$ are different.

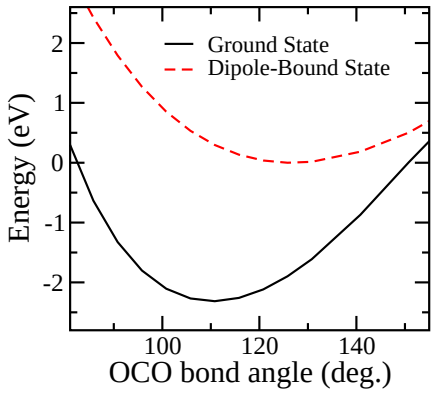

FIG. 7: (Color online) Potential energy surfaces of ground state trans-$HOCO^-$ and dipole bound trans-$HOCO^-$ along OCO bend.

Fig. 7 shows a cut through the latter two surfaces, calculated using the CISD method, along the OCO bend which shows that the OCO angles, at equilibrium, are different. Here the geometry of the molecule other than the quantity being plotted is frozen at the equilibrium geometry of the ground-state anion. A full optimization of the dipole-bound anion geometry would lower the upper curve in Fig. 7 by ∼1 eV. If we make a Frank-Condon approximation using these potentials, we see that an appreciably nonzero Franck-Condon factor for the transition from the ground state of $HOCO^-$ to the third OCO bending level of the dipole-bound anion is to be expected.

We must also verify that the dipole bound anion potential surface can support vibrational states of the relevant bending mode up to $\nu = 2$. Fig. 8a shows a cut through the potential energy surfaces of the HOCO radical and dipole-bound $HOCO^-$. The bond parameters, other than the ones plotted, are frozen at the equilibrium values of the radical given in ref. [6]. As expected, the potential energy surfaces of the two species are essentially identical. The OCO bend vibrational energy levels, ν_f are also shown in the figure and they are derived from the experimental IR frequency[43]. The binding energy of the anion and the dipole moment of the radical along the OCO bend are plotted in Fig 8b and 8c, respectively. They demonstrate the sensitivity of the binding energy to the dipole moment of the molecule. As the OCO bond angle increases, the permanent dipole moment of the molecule decreases and as a result the anion becomes less bound. The potential energy surfaces of the two states cross when the OCO bond angle is 141.1 degrees, which is energetically just above ν_f=2 vibrational state. The crossing of the states is represented by the vertical line in the figure. E_{bind}=0 is represented by the horizontal line in Fig. 8b. According to these calculations, the dipole-bound anion can support three OCO bending vibrational levels for which classically allowed motion occurs exclusively at angles where the state is electronically

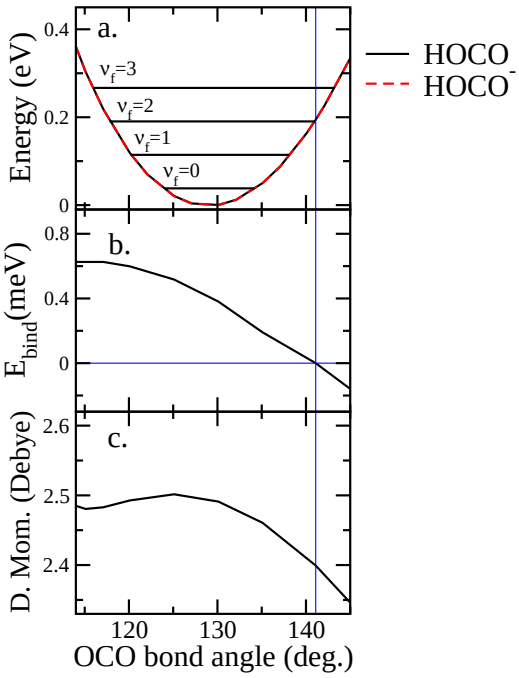

FIG. 8: (Color online) a). Potential energy surfaces of trans-HOCO radical and dipole bound trans-$HOCO^-$ along the OCO bend. The change in b) binding energy and c) dipole moment along the bend is also plotted.

bound, and the highest of these is the one that this mechanism suggests is responsible for the threshold peaks.

Finally, we must ask whether an alternate, simpler mechanism might produce these threshold peaks in the photoelectron spectrum. Direct photodetachment leaving neutral HOCO in vibrationally excited states is certainly such a mechanism, and essentially the same Franck-Condon analysis given above would apply to direct photodetachment. For example, a vibrational progression is seen in the photodetachment spectrum of the nitromethane anion [25], which has no known dipole bound states. If the two prominent threshold peaks seen in the experiment Lu and Continetti [8] were the beginning of such a progression, then experiments with higher photon energies should contain those two peaks and perhaps also additional members of the progression. However, such features are not seen in experiments with 3.21 eV photons by Lu et al. [7] or in experiments with 4.8 eV photons by Clements et al. [6]. By the same token, if our interpretation is correct, then an experiment carried out at a photon frequency ∼0.1 eV lower than the 1.6 eV that was previously used should yield only one threshold peak.

IV. SUMMARY

We have argued that the two peaks observed in the threshold photodetachment spectrum of $HOCO^-$ do not

imply the existence of low-energy s- and p- wave shape resonances, but rather result from the decay of a vibrational excited state of the dipole-bound anion into lower states of the HOCO neutral. Our conclusions are based on a series of electronic structure calculations, as well as fixed-nuclei electron - HOCO scattering calculations. The dipole moment of the trans-radical computed at the MP2 level of theory is 2.84 Debye, which is larger than the threshold value that Garret[40] suggests is needed to bind an electron. Furthermore, our CISD calculation using diffuse sets of basis functions, predicts the binding energy of the dipole-bound anion to be 0.48 meV. Our complex Kohn calculations also predict an $A''(\pi)^*$ shape resonance several electron volts above the photodetachment threshold. A partial wave analysis shows that this resonance is characterized by predominant l=1 and l=2 components. Finally, we have calculated laboratory frame photoelectron angular distributions. In the threshold region, they agree with the distributions measured by Lu and Continetti[8]. Experimental verification of the dipole bound state mechanism might be found in an experiment performed with a tunable source, such as those that have observed such resonances in enolates[16, 44].

Acknowledgments

This work was performed under the auspices of the US Department of Energy by the University of California Lawrence Berkeley National Laboratory under Contract DE-AC02-05CH11231 and was supported by the U.S. DOE Office of Basic Energy Sciences, Division of Chemical Sciences. AEO acknowledges support from the National Science Foundation (Grant No. PHY-05-55401).

[1] J. A. Miller, R. J. Kee, and C. K. Westbrook, Annu. Rev. Phys. Chem. **41**, 313–344 (1990).
[2] F. N. Dzegilenko and J. M. Bowman, J. Chem. Phys. **105**, 2280–2286 (1996).
[3] T. Röckmann, C. A. M. Brenninkmeijer, G. Saueressig, P. Bergamaschi, J. N. Crowley, H. Fischer, and P. J. Crutzen, Science **281**, 544–546 (1998).
[4] D. A. Dixon, D. Feller, and J. S. Francisco, J. Phys. Chem. A **107**, 186–190 (2003).
[5] S. Zhang, D. M. Medvedev, E. M. Goldfield, and S. K. Gray, J. Chem. Phys. **125**, 164312 (2006).
[6] T. G. Clements, R. E. Continetti, and J. S. Francisco, J. Chem. Phys. **117**, 6478–6488 (2002).
[7] Z. Lu, Q. Hu, J. E. Oakman, and R. E. Continetti, J. Chem. Phys. **126**, 194305 (2007).
[8] Z. Lu and R. E. Continetti, Phys. Rev. Lett. **99**, 113005 (2007).
[9] J.-M. Lévy-Leblond, Phys. Rev. **153**, 1–4 (1967).
[10] N. F. Lane, Rev. Mod. Phys. **52**, 29 (1980).
[11] J. Simons and K. D. Jordan, Chem. Rev. **87**, 535 (1987).
[12] K. Rohr and F. Linder, J. Phys. B **8**, L200 (1975).
[13] K. Rohr and F. Linder, J. Phys. B **9**, 2521 (1976).
[14] A. H. Zimmerman and J. I. Brauman, J. Chem. Phys. **66**, 5823–5825 (1977).
[15] R. L. Jackson, A. H. Zimmerman, and J. I. Brauman, J. Chem. Phys. **71**, 2088–2094 (1979).
[16] R. D. Mead, K. R. Lykke, W. C. Lineberger, J. Marks, and J. I. Brauman, J. Chem. Phys. **81**, 4883–4892 (1984).
[17] M. Sindelka, V. Spirko, P. Jungwirth, F. Wang, S. Mahalakshmi, and K. D. Jordan, J. Chem. Phys. **121**, 1824–1829 (2004).
[18] V. E. Chernov, A. V. Dolgikh, and B. A. Zon, Phys. Rev. A **72**, 052701 (2005).
[19] B. Boudaïffa, P. Cloutier, D. Hunting, M. A. Huels, and L. Sanche, Science **287**, 1658–1660 (2000).
[20] G. Hanel, B. Gstir, S. Denifl, P. Scheier, M. Probst, B. Farizon, M. Farizon, E. Illenberger, and T. D. Märk, Phys. Rev. Lett. **90**, 188104 (2003).
[21] S. Denifl, S. Ptasinska, M. Cingel, S. Matejcik, P. Scheier, and T. D. Mrk, Chem. Phys. Letts. **377**, 74 – 80 (2003).
[22] A. M. Scheer, K. Aflatooni, G. A. Gallup, and P. D. Burrow, Phys. Rev. Lett. **92**, 068102 (2004).
[23] R. W. Wetmore, H. F. Schaefer, P. C. Hiberty, and J. I. Brauman, JACS **102**, 5470–5473 (1980).
[24] M. Gutowski, P. Skurski, A. I. Boldyrev, J. Simons, and K. D. Jordan, Phys. Rev. A **54**, 1906–1909 (1996).
[25] R. N. Compton, J. H. S. Carman, C. Desfrancois, H. Abdoul-Carime, J. P. Schermann, J. H. Hendricks, S. A. Lyapustina, and K. H. Bowen, J. Chem. Phys. **105**, 3472–3478 (1996).
[26] P. Skurski, M. Gutowski, and J. Simons, J. Chem. Phys. **114**, 7443–7449 (2001).
[27] F. Wang and K. D. Jordan, J. Chem. Phys. **114**, 10717–10724 (2001).
[28] M. Gutowski, C. S. Hall, L. Adamowicz, J. H. Hendricks, H. L. de Clercq, S. A. Lyapustina, J. M. Nilles, S.-J. Xu, and K. H. Bowen, Phys. Rev. Lett. **88**, 143001 (2002).
[29] W. Kohn, Phys. Rev. **74**, 1763 (1948).
[30] T. N. Rescigno, B. H. Lengsfield, and C. W. McCurdy, in *Modern Electronic Structure Theory*, edited by D. R. Yarkony (World Scientific, Singapore, 1995), Vol. 1.
[31] T. N. Rescigno and A. E. Orel, Phys. Rev. A **43**, 1625 (1991).
[32] T. H. Dunning, Journal of Chemical Physics **53**, 2823 (1970).
[33] J. C. Slater, *The Self-Consistent Field for Molecules and Solids* (McGraw-Hill, New York, 1974), Vol. 4.
[34] N. Saito, A. De Fanis, K. Kubozuka, M. Machida, M. Takahashi, H. Yoshida, I. H. Suzuki, A. Cassimi, A. Czasch, L. Schmidt, R. Döner, K. Wang, B. Zimmermann, V. McKoy, I. Koyano, and K. Ueda, Journal of Physics B: Atomic, Molecular and Optical Physics **36**, L25 (2003).
[35] X.-J. Liu, H. Fukuzawa, T. Teranishi, A. De Fanis, M. Takahashi, H. Yoshida, A. Cassimi, A. Czasch, L. Schmidt, R. Dörner, K. Wang, B. Zimmermann, V. McKoy, I. Koyano, N. Saito, and K. Ueda, Phys. Rev. Lett. **101**, 083001 (2008).
[36] S. Miyabe, C. W. McCurdy, A. E. Orel, and T. N. Rescigno, Phys. Rev. A **79**, 053401 (2009).
[37] K. Zähringer, H.-D. Meyer, and L. S. Cederbaum, Phys.

Rev. A **45**, 318–328 (1992).
[38] J. Schirmer, M. Braunstein, and V. McKoy, Phys. Rev. A **41**, 283–300 (1990).
[39] E. Fermi and E. Teller, Phys. Rev. **72**, 399–408 (1947).
[40] W. R. Garret, Journal of Chemical Physics **77**, 3666 (1982).
[41] C. Desfrancois, H. Abdoul-Carime, N. Khelifa, and J. P. Schermann, Phys. Rev. Lett. **73**, 2436–2439 (1994).
[42] M. J. Frisch *et al.*, Gaussian 09 Revision A.1, gaussian Inc. Wallingford CT 2009.
[43] M. E. Jacox, *Vibrational and Electronic Energy Levels of Polyatomic Transient Molecules* (American Institute of Physics, New York, 1994), Vol. 4.
[44] E. A. Brinkman, S. Berger, J. Marks, and J. I. Brauman, The Journal of Chemical Physics **99**, 7586–7594 (1993).